

Field-free spin-orbit switching of canted magnetization in Pt/Co/Ru/RuO₂(101) multilayers

Yunzhuo Wu¹, Tong Wu¹, Haoran Chen¹, Yongwei Cui¹, Hongyue Xu¹, Nan Jiang¹,
Zhen Cheng¹, Yizheng Wu^{1,2,3,*}

¹*Department of Physics and State Key Laboratory of Surface Physics, Fudan University,
Shanghai 200433, China*

²*Shanghai Research Center for Quantum Sciences, Shanghai 201315, China*

³*Shanghai Key Laboratory of Metasurfaces for Light Manipulation, Fudan University, Shanghai
200433, China*

Abstract

Enabling field-free current-induced switching of perpendicular magnetization is essential for advancing spin-orbit-torque magnetic random access memory technology. Our research on the Pt/Co/Ru/RuO₂(101) system has successfully demonstrated field-free switching through current injection along the RuO₂[010] axis. We discovered that the system exhibits a tilted easy axis, inclined from the out-of-plane towards the RuO₂[$\bar{1}01$] direction. The application of current perpendicular to this tilted axis generates a substantial out-of-plane effective field, which facilitates field-free magnetization switching. Our results also indicate that adjusting the thickness of the Ru layer to optimize the tilt angle can significantly reduce the critical switching current density. This work provides a viable strategy for controlling the tilting magnetization, essential for the development of RuO₂-based magnetic devices.

Spin-orbit torque (SOT) is a crucial technology for the next-generation magnetic random access memory (MRAM), facilitating efficient manipulation of magnetization in spintronic devices^{1,2}. The pursuit of low writing current density, minimal power consumption, and nonvolatility through full electrical control is central to SOT-MRAM research. The manipulation of magnetization via SOT typically depends on spin currents generated by substantial spin-orbit coupling (SOC) in heavy metals (HMs). Achieving SOT switching of magnetization with perpendicular magnetic anisotropy (PMA) has typically required an external magnetic field aligned with the current direction to break the symmetry^{3,4}. This necessity for an additional in-plane field poses a challenge for practical device applications. Various innovative methods have been explored to facilitate field-free magnetization switching⁵⁻⁸. These include breaking the structural and magnetic symmetry in samples with wedge-shaped structure^{9,10}, utilizing a gradient oxidized capping layer⁸, and employing exchange bias¹¹⁻¹⁴. Moreover, the out-of-plane SOT can be induced in materials with broken symmetry, such as WTe₂¹⁵, Mn₂Au¹⁶ and CuPt/CoPt bilayers^{17,18}, when the current is injected along the low-symmetry axis of the nonmagnetic layers. These strategies are crucial steps towards the development of more efficient and versatile SOT-MRAM devices.

RuO₂, with its rutile crystal structure, is an emerging antiferromagnetic material that has garnered attention in the field of spintronics. The spin-splitting effect (SSE) in RuO₂, which results from its spin-splitting band, has been theoretically predicted and remains a subject of ongoing research¹⁹⁻²¹. When a charge current is injected, the spin polarization induced by the SSE is found to align with the Néel vector direction of RuO₂²²⁻²⁴. The anisotropic SSE has been experimentally observed using the spin-torque ferromagnetic resonance method, which confirmed the presence of a spin current with polarization along the z-direction (σ_z)^{22,23}. S. Karube et al. have reported the field-free magnetization switching behavior in the Pt/Co/Ru/RuO₂(101) multilayer stacks²². Additionally, in the Ru/Pt/Co/Pt/RuO₂(101) heterostructures, robust field-free switching can be realized induced by spin current with σ_z ²⁵. However, recent muon spin rotation and relaxation experiments suggested that bulk RuO₂ behaves as a non-magnetic metal²⁶. Additionally, Z.Q. Wang et al. reported that the anisotropic inverse

spin Hall effect is the dominant mechanism for spin-charge conversion in the RuO₂(101) films²⁷. These findings raise questions about whether the field-free switching behavior observed in the Pt/Co/Ru/RuO₂(101) system is indeed induced by the SSE. Therefore, further intensive research is necessary to investigate the origin of the field-free SOT-induced magnetization switching in RuO₂-based magnetic systems.

In this letter, we systematically investigated the field-free magnetization switching behavior in RuO₂-based magnetic system. We fabricated a Pt/Co/Ru multilayer exhibiting PMA on the RuO₂(101) plane. Consistent field-free switching can be achieved for the current injected along the RuO₂[010] direction. Our detailed analysis revealed that the magnetic easy axis is not aligned perpendicularly to the plane but is instead tilted, with its in-plane component oriented towards RuO₂[$\bar{1}01$] direction. This observation suggests that the field-free switching in this structure is predominantly due to the presence of this tilted easy axis. Additionally, measurements under direct current (DC) conditions indicate that the out-of-plane effective field is significant for the current injecting along the [010] direction, while it is almost negligible for the current injecting along the [$\bar{1}01$] direction. Furthermore, it was discovered that optimizing the tilt angle by adjusting the thickness of the Ru layer can significantly reduce the critical switching current density. This reduction is approximately one order of magnitude lower than that typically observed in Co/Pt systems^{3,12,28}. These results provide valuable insights into the mechanisms underlying field-free magnetization switching in RuO₂-based systems and have significant implications for the development of advanced magnetic devices.

The Pt/Co/Ru/RuO₂ films were grown on Al₂O₃(1 $\bar{1}02$) substrates in a magnetron sputtering system with a base pressure of 2×10^{-8} Torr²⁹. The sapphire substrates were pre-annealed at 500°C for 1 hour in the vacuum chamber to prepare the surface for deposition. The RuO₂ films were epitaxially deposited through reactive sputtering in an oxygen-argon atmosphere of 3 mTorr, with a ratio of 1:4. Subsequent layers were deposited under an argon pressure of 3 mTorr at room temperature.

X-ray diffraction measurements confirmed the formation of a single crystalline RuO₂(101) film^{22,29}. To systematically investigate the impact of the intermediate Ru

layer on SOT switching, a wedge-shaped Ru layer was introduced, facilitating a gradual change in Ru thickness. The thickness gradient, spanning from 0 to 1.2 nm at a rate of ~ 0.2 nm/mm, was controlled by moving a shutter over the substrate during deposition. Additionally, a thick Ru layer with a thickness of 6.2 nm was also grown as a shoulder on the same sample.

For the electrical measurements, the samples were patterned into Hall bar devices using standard photolithography and Ar⁺ ion milling techniques. Each device has dimensions of 15 μm in width and 100 μm in length. During the current-induced magnetization switching measurements, a 100 μs current pulse was applied into the Hall bar devices. After each pulse, the Hall resistance was measured 1 second later using a small DC current of 1 mA. A commercial magneto-optic Kerr microscope from Evico Magnetics GmbH was used to investigate the evolution of the magnetic domain images excited by the current pulses^{30,31}. To further ascertain the tilt angle and anisotropy field, anomalous Hall effect (AHE) measurements were conducted by varying the magnetic field direction in a superconducting vector magnet system.

The current-induced magnetization switching measurements were initially conducted on a Pt(2 nm)/Co(0.8 nm)/Ru(0.8 nm)/RuO₂(8 nm) multilayer stack, which mirrors the sample structure reported in Ref. 22. Fig. 1(a) presents the simultaneous measurement setup for Hall voltage signals and magnetic domain images captured through Kerr microscopy. The presence of PMA in the sample was verified by the characteristic out-of-plane hysteresis loop shown in Fig. 1(b).

Subsequently, the behavior of current-driven magnetization switching under zero external field was investigated. Fig. 1(c) illustrates a clear field-free switching behavior when the current was applied along the [010] direction ($I//\text{RuO}_2[010]$), with no switching observed for $I//\text{RuO}_2[\bar{1}01]$. Fig. 1(d) displays the domain images post-application of 32 mA current pulses along the [010] direction, which clearly depict full switching at zero field. Thus, the deterministic field-free switching in the Pt/Co/Ru/RuO₂(101) system can be conclusively demonstrated, consistent with the results reported in Ref. 22²².

Fig. 1(e) displays the typical current-induced magnetization switching loops under

varying in-plane field strengths for the current directed along the [010] direction. The switching polarity consistently follows a counterclockwise direction, with no changes in polarity for the field up to -1000 Oe. In most systems exhibiting field-free magnetization switching, the switching polarity can be altered with the in-plane field strength exceeding a certain threshold, typically no more than approximately 500 Oe^{9,10,32-34}. Thus, our measurements indicate that the magnetization switching in the Pt/Co/Ru/RuO₂ system is notably resilient to external field disturbances.

Usually, field-free switching in RuO₂-based magnetic systems is attributed to the spin-splitter effect²². However, in the Py/RuO₂(101) system with PMA, field-free magnetization switching is not observed despite the expected presence of the spin-splitter effect³⁵. It is noteworthy that the hysteresis loop depicted in Fig. 1(b) shows no saturation in the AHE signal after magnetization switching, suggesting that the easy axis is tilted away from the z-axis. It has been reported that field-free switching is feasible in systems exhibiting tilted anisotropy when a current is applied perpendicular to the tilted axis^{9,36,37}. Therefore, the orientation of the magnetic easy axis and its influence on field-free switching were further investigated.

We subsequently conducted measurements of the hysteresis loop over a broader field range. Fig. 2(a) clearly shows that the Hall signal (R_H) saturates at fields exceeding 15 kOe, and the inset R_H loop under the narrow field range exhibits a shape similar to that in Fig. 1(b). This finding unequivocally indicates that the magnetization at zero field is not aligned perpendicularly to the film plane but is inclined from the normal direction. By determining the ratio of the remanent value (R_{Rem}) at zero field to the saturation value (R_{Sat}), it was deduced that the easy axis is inclined at an angle of approximately 66° from the z-axis.

The R_H measurements are only sensitive to the z-component of magnetization, which is insufficient to ascertain the in-plane orientation of the easy axis. Thus, we proceeded to measure the hysteresis loops with fields applied in different directions utilizing a superconducting quantum interference device (SQUID). Fig. 2(b) displays the in-plane and out-of-plane magnetization hysteresis (M-H) loops. The inset indicates the presence of remanent magnetization in both the $[\bar{1}01]$ direction and the z-direction, yet the

absence in the [010] direction. The remanent magnetization along the $[\bar{1}01]$ direction surpasses that along the z-direction, implying that the easy axis of the magnetic moment deviates from the z-axis towards the $[\bar{1}01]$ direction, as depicted in Fig. 2(c).

Both experimental evidence and theoretical models have confirmed that field-free switching is achievable in systems with a tilted easy axis^{7,9,36-38}. This type of switching is facilitated for the current injected perpendicular to the tilted axis. In the system under investigation, the in-plane component of the tilted magnetization is oriented along the $[\bar{1}01]$ direction, and field-free switching is observed for $I//\text{RuO}_2[010]$ (Fig. 1(c)). Thus, we conclude that the field-free switching in this system is primarily driven by the tilting of the easy axis, suggesting that the SSE may not significantly contribute to the observed field-free switching behavior. It is noted that the ultrathin Py film grown on $\text{RuO}_2(101)$ surface also exhibits strong PMA, yet no field-free switching is detected³⁵, which further supports the notion that the SSE in $\text{Pt/Co/Ru/RuO}_2(101)$ system does not play a crucial role in the current-induced magnetization switching.

In the magnetic system with a tilted easy axis, it is well-documented that an out-of-plane effective field can be induced by the current injected perpendicular to the tilted axis^{7,9,36,37}. However, when current is injected parallel to the tilted axis, no significant out-of-plane effective field can be observed. To evaluate the out-of-plane effective field induced by SOT on the tilted magnetization, we performed the hysteresis loop measurements with varying DC current strengths^{13,17,18}.

Figs. 3(a) and (b) depict the typical hysteresis loops under different currents for $I//\text{RuO}_2[010]$ and $I//\text{RuO}_2[\bar{1}01]$, respectively. At currents below 15 mA, the hysteresis loops for both current polarities are identical, suggesting the absence of a notable out-of-plane effective field. At a current of 17 mA with $I//\text{RuO}_2[010]$, the hysteresis loop shifts completely to the left for positive current and to the right for negative current. This shift indicates the presence of an out-of-plane effective field, which serves as the driving force for the observed deterministic field-free switching. It is noted that the current-induced switching in Fig. 1(c) requires a significantly higher current strength above 24 mA for pulsed current, potentially due to disparate heating effects under DC and pulsed current conditions. In contrast, for the case with 17 mA current applied along

the $[\bar{1}01]$ direction, as shown in Fig. 3(b), the hysteresis loops for both positive and negative currents are similar, indicating a minimal out-of-plane effective field. This is in line with the observation that field-free switching does not occur for $I//\text{RuO}_2[\bar{1}01]$.

Fig. 3(c) presents the current-dependent coercivities (H_c) of the hysteresis loops for both current directions. The H_c exhibit a similar decline with current for $I < 15$ mA, which is attributable to the effect of Joule heating. However, beyond 15 mA, the H_c for $I//\text{RuO}_2[010]$ is markedly lower than that for $I//\text{RuO}_2[\bar{1}01]$. This disparity is due to the influence of the current-induced effective field. Fig. 3(d) illustrates the shift field H_{shift} as a function of current. For $I//\text{RuO}_2[010]$, H_{shift} exhibits opposite signs for opposite current directions when the current exceeds 15 mA. The maximum measurable H_{shift} is observed to reach 100 Oe at a current of 17 mA. In contrast, for $I//\text{RuO}_2[\bar{1}01]$, H_{shift} remains negligible across all applied current levels.

We have further quantified the out-of-plane effective field H_z^{eff} as a function of the averaged current density, as depicted in the inset of Fig. 3(d). H_z^{eff} is determined by averaging the H_{shift} under positive and negative currents, i.e. $H_z^{\text{eff}} = |H_{\text{shift}}(+I) - H_{\text{shift}}(-I)|/2$. The current density is derived by dividing the current by the total cross-sectional area of the multilayer stack. At a current of 17 mA, the average current density is $9.7 \times 10^{10} \text{ A/m}^2$, which generates H_z^{eff} of 100 Oe. Consequently, the out-of-plane SOT efficiency is calculated to be $\chi = H_z^{\text{eff}}/J = 103 \text{ Oe}/10^{11} \text{ Am}^{-2}$. This efficiency significantly exceeds the previously determined values of $3 \text{ Oe}/10^{11} \text{ Am}^{-2}$ in the Pt/Co/Pt system⁹, and $56 \text{ Oe}/10^{11} \text{ Am}^{-2}$ in the TaO_x/CoFeB/Ta system⁸.

It is important to note that current densities in the RuO₂ layer and other metal layers may vary due to different resistivities across layers. In Ref. 22, the determined resistivity is $160 \mu\Omega \text{ cm}$ in the Pt layer and $55 \mu\Omega \text{ cm}$ in the RuO₂ layer. The higher resistivity and the thinner thickness of the Pt layer implies a relatively higher current density in RuO₂, suggesting that the RuO₂ layer is the primary contributor to the spin current. Assuming that the resistivities of the Ru and Co ultrathin layers are similar to that of the Pt layer, the estimated out-of-plane SOT efficiency due to the current in the RuO₂ layer is approximately to be $65 \text{ Oe}/10^{11} \text{ Am}^{-2}$, which is still larger than the reported values in other systems^{8,9,17}. Furthermore, considering that the Co/Pt system

exhibits the same polarity of current-induced switching as observed in the current Pt/Co/Ru/RuO₂ system³⁷, the top Pt layer is expected to have an SOT effect opposite to that of the bottom RuO₂ layer. In the Pt/Co/Pt/RuO₂ structure in Ref. 25, the upper and lower layers of Pt are of equal thickness, suggesting that the spin current generated by Pt cancels out²⁵. The switching behavior induced by the RuO₂ is also consistent with our findings. So, the RuO₂ layer could possess a very strong SOT effect, highlighting its critical role in the field-free switching performance in this system.

Next, we focus on the role of the Ru interlayer on the field-free switching. Our experiments revealed that a Pt/Co bilayer directly grown on the RuO₂ surface exhibits only in-plane anisotropy. This observation suggests that the Ru interlayer is instrumental in enhancing the PMA in our system. Moreover, the crystal structure of RuO₂(101) film shows the mirror-symmetry broken along the $[\bar{1}01]$ direction, thus inducing the tilted magnetic anisotropy. It is hypothesized that the tilted magnetic anisotropy varies with the Ru thickness d_{Ru} . To delve deeper into the relationship between field-free switching and the angle of the tilted easy axis, we systematically varied d_{Ru} by growing a wedge-shaped Ru layer. This approach enabled us to continuously modulate the tilt angle of the Co magnetic moment, as shown in Fig. 4(a). A series of Hall bar devices with varying d_{Ru} were fabricated on the wedge-shaped sample. To ascertain the tilt angle Θ of the easy axis and the magnetic anisotropy field for different d_{Ru} , we employed the AHE measurements with a rotating field in Hall bar devices. This technique is grounded in the principle of magnetic torqueometry, and provides a precise method of measuring the magnetic anisotropy and the orientation of the easy axis in our samples^{39,40}.

Fig. 4(b) displays the θ_{H} -dependent R_{H} curves for different d_{Ru} by rotating the magnetic field, which is maintained at a fixed strength of 15 kOe. The field rotation is conducted in the plane containing the z-axis and the $[\bar{1}01]$ direction, with θ_{H} representing the field angle, as depicted in the inset of Fig. 4(b). In the $R_{\text{H}}(\theta_{\text{H}})$ curves for systems with $d_{\text{Ru}} = 0.53$ nm and 0.98 nm, the angles corresponding to the maximum R_{H} signals clearly deviate from 0 and 180°. This deviation indicates that the easy axis is tilted away from the z-axis. The measured $R_{\text{H}}(\theta_{\text{H}})$ curve for $d_{\text{Ru}} = 0$ nm exhibits

symmetry around 180° , affirming that its easy axis resides in the film plane, as confirmed by subsequent fitting analyses.

The R_H signal is known to be proportional to the z-component of magnetization, i. e. $R_H \propto \cos\theta_m$, which allows us to establish the relationship between the magnetization angle θ_m and the field angle θ_H ^{35,39-41}. Then, the anisotropy torque field $\tau(\theta_m)$ can be determined as a function of θ_m by the formula $\tau(\theta_m) = H \sin(\theta_H - \theta_m) = H_k \sin(2(\theta_m - \Theta))$ ³⁹⁻⁴¹. The uniaxial anisotropy field H_k and the tilt angle Θ of the magnetic anisotropy can be extracted through fitting the $\tau(\theta_m)$ curve (not shown here). As depicted in Fig. 4(c), the tilt angle gradually changes from 90° to 69° as d_{Ru} increases from 0 nm to 1 nm, and then it gradually decreases for thicker Ru layers, reaching 65° at $d_{Ru}=6.2$ nm. Fig. 4(d) shows that H_k increases steadily with d_{Ru} , thereby demonstrating a continuous decrease in H_k with the increasing tilt angle Θ , as depicted in the inset of Fig. 4(d).

We further performed the out-of-plane R_H -loop measurements for the Hall devices with varying Ru thicknesses. Fig. 4(e) shows that all loops for $d_{Ru} > 0$ nm exhibit noticeable jumping behavior under a small magnetic field, and the coercivity H_c gradually increases with d_{Ru} , as shown in Fig. 4(f). The remanent signals in R_H loops show clear increase with the film thickness, and the saturation signals in Fig. 4(b) have the similar value, thus the hysteresis loop measurements also indicate the z-component of magnetization increase with d_{Ru} .

To elucidate the impact of the tilted anisotropy on field-free switching, we performed the current-induced magnetization switching measurements at zero field with $I//RuO_2[010]$. As shown in Fig. 4(g), all Hall devices with different d_{Ru} in the wedge-shaped sample, excluding those at $d_{Ru}=0$ nm and $d_{Ru}=6.2$ nm, demonstrate clear field-free switching behavior. By examining the current-induced resistance changes in conjunction with the remanence R_H signals in hysteresis loop presented in Fig. 4(e), we can ascertain that complete magnetization switching is attainable for all the samples illustrated in Fig. 4(g). This comparison highlights the pivotal role of the tilted anisotropy in enabling efficient field-free switching in these devices.

The current-induced switching measurements depicted in Fig. 4(g) also reveal a

significant variation in the critical switching current, which is notably low at 3.5 mA for the device with $d_{\text{Ru}}=0.18$ nm. Fig. 4(h) presents the critical switching current density J_{sw} as a function of d_{Ru} , exhibiting an order of magnitude change as d_{Ru} increases from 0.18 nm to 1.2 nm. The minimum J_{sw} is only $2.2 \times 10^{10} \text{ A/m}^2$ observed in the device with $d_{\text{Ru}}=0.18$ nm, which has the tilt angle Θ of 85° . Even when accounting for the shunting effect due to different resistivities across layers, the critical switching current density in this system remains an order of magnitude lower than that typically found in most Pt/Co systems^{3,12,28}.

This reduced critical switching current density can be ascribed to several factors. Firstly, the anisotropy field strength is considerably lower in devices with a thinner Ru layer, as evidenced in Fig. 4(d). Secondly, the presence of a thin Ru layer between Co and RuO₂ may diminish the spin current originating from the RuO₂ layer due to the short diffusion length within the Ru layer⁴², suggesting that the spin current may have higher transmission in devices with a thinner Ru layer. It is noteworthy that field-free switching is not observed in the device with a 6.2 nm Ru interlayer, despite the magnetic anisotropy being closely comparable to that of devices with a 1.2 nm Ru interlayer. This finding further supports that a strong spin current is generated from the RuO₂ layer but can be obstructed by a thick Ru layer.

Moreover, it should be noted that the conventional spin current with polarization along the y-direction (σ_y) continues to significantly influence current-induced magnetization switching, particularly in devices with current applied along the RuO₂[010] direction with in-plane fields. To date, there is a relative scarcity of research on the interplay between σ_y and σ_z on the current-induced switching. Our study suggests that controlling the magnetization tilting could offer a valuable strategy to optimize current-induced switching, which is crucial for the development of next-generation SOT-MRAM devices.

In summary, we demonstrated that the Pt/Co/Ru multilayers grown on RuO₂(101) can realize the field-free current induced magnetization switching for the current injecting in RuO₂[010] direction. Our magnetic measurements revealed that the Co layer exhibits a magnetic anisotropy easy axis tilted towards the $[\bar{1}01]$ direction. The

observed field-free switching behavior is primarily attributed to this tilted magnetic easy axis, which can generate a significant out-of-plane effective field when current is applied along the RuO₂[010] direction. In addition, by adjusting the thickness of the inserted Ru layer, we can control the tilt angle of the easy axis. We achieved the field-free switching at a low current density of $2.2 \times 10^{10} \text{ A/m}^2$ at a tilt angle of 85. The ability to control the tilt angle of the easy axis and achieve low current density switching represents a significant step towards the practical application of these systems in next-generation spintronic devices. Our findings not only offer insights into the mechanisms of field-free switching in RuO₂-based magnetic systems but also pave the way for developing more efficient and reliable magnetic memory devices.

The work was supported by the National Key Research and Development Program of China (2022YFA1403300), the National Natural Science Foundation of China (Grant No. 11974079, No. 12274083, and No. 12174028), the Shanghai Municipal Science and Technology Major Project (Grant No. 2019SHZDZX01), and the Shanghai Municipal Science and Technology Basic Research Project (Grant No. 22JC1400200 and No. 23dz2260100).

Data Availability Statement

The data that support the findings of this study are available from the corresponding author upon reasonable request.

* wuyizheng@fudan.edu.cn

References

- ¹ S. Ikeda, K. Miura, H. Yamamoto, K. Mizunuma, H. D. Gan, M. Endo, S. Kanai, J. Hayakawa, F. Matsukura, and H. Ohno, "A perpendicular-anisotropy CoFeB–MgO magnetic tunnel junction", *Nat. Mater.* **9**, 721 (2010).
- ² J.-M. Hu, Z. Li, L.-Q. Chen, and C.-W. Nan, "High-density magnetoresistive random access memory operating at ultralow voltage at room temperature", *Nat. Commun.* **2**, 553 (2011).
- ³ L. Liu, O. J. Lee, T. J. Gudmundsen, D. C. Ralph, and R. A. Buhrman, "Current-induced switching of perpendicularly magnetized magnetic layers using spin torque from the spin Hall effect", *Phys. Rev. Lett.* **109**, 096602 (2012).
- ⁴ I. M. Miron, K. Garello, G. Gaudin, P.-J. Zermatten, M. V. Costache, S. Auffret, S. Bandiera, B. Rodmacq, A. Schuhl, and P. Gambardella, "Perpendicular switching of a single ferromagnetic layer induced by in-plane current injection", *Nature* **476**, 189 (2011).
- ⁵ T.-Y. Chen, H.-I. Chan, W.-B. Liao, and C.-F. Pai, "Current-induced spin-orbit torque and field-free switching in Mo-based magnetic heterostructures", *Phys. Rev. Appl.* **10**, 044038 (2018).
- ⁶ M. Akyol, G. Yu, J. G. Alzate, P. Upadhyaya, X. Li, K. L. Wong, A. Ekicibil, P. Khalili Amiri, and K. L. Wang, "Current-induced spin-orbit torque switching of perpendicularly magnetized Hf[CoFeB|MgO and Hf[CoFeB|TaOx structures", *Appl. Phys. Lett.* **106** (2015).
- ⁷ T. Li, W. Luo, J. Wu, X. Li, H. Yang, X. Zhao, and H. An, "Field-free magnetization switching with full scale in Pt/Tm₃Fe₅O₁₂ bilayer on vicinal substrate", *Appl. Phys. Express* **17**, 033003 (2024).
- ⁸ G. Yu, P. Upadhyaya, Y. Fan, J. G. Alzate, W. Jiang, K. L. Wong, S. Takei, S. A. Bender, L.-T. Chang, Y. Jiang, M. Lang, J. Tang, Y. Wang, Y. Tserkovnyak, P. K. Amiri, and K. L. Wang, "Switching of perpendicular magnetization by spin–orbit torques in the absence of external magnetic fields", *Nat. Nanotechnol.* **9**, 548 (2014).
- ⁹ V. M. P, K. R. Ganesh, and P. S. A. Kumar, "Spin Hall effect mediated current-induced deterministic switching in all-metallic perpendicularly magnetized Pt/Co/Pt trilayers", *Phys. Rev. B* **96**, 104412 (2017).
- ¹⁰ X. Shu, L. Liu, J. Zhou, W. Lin, Q. Xie, T. Zhao, C. Zhou, S. Chen, H. Wang, J. Chai, Y. Ding, W. Chen, and J. Chen, "Field-free switching of perpendicular magnetization induced by longitudinal spin-orbit-torque gradient", *Phys. Rev. Appl.* **17**, 024031 (2022).
- ¹¹ S. Fukami, C. Zhang, S. DuttaGupta, A. Kurenkov, and H. Ohno, "Magnetization switching by spin–orbit torque in an antiferromagnet–ferromagnet bilayer system", *Nat. Mater.* **15**, 535 (2016).
- ¹² A. van den Brink, G. Vermeijs, A. Solignac, J. Koo, J. T. Kohlhepp, H. J. M. Swagten, and B. Koopmans, "Field-free magnetization reversal by spin-Hall effect and exchange bias", *Nat. Commun.* **7**, 10854 (2016).
- ¹³ S.-h. C. Baek, V. P. Amin, Y.-W. Oh, G. Go, S.-J. Lee, G.-H. Lee, K.-J. Kim, M. D. Stiles, B.-G. Park, and K.-J. Lee, "Spin currents and spin–orbit torques in ferromagnetic trilayers", *Nat. Mater.* **17**, 509 (2018).
- ¹⁴ Y.-W. Oh, S.-h. Chris Baek, Y. M. Kim, H. Y. Lee, K.-D. Lee, C.-G. Yang, E.-S. Park, K.-S. Lee, K.-W. Kim, G. Go, J.-R. Jeong, B.-C. Min, H.-W. Lee, K.-J. Lee, and B.-G. Park, "Field-free switching of perpendicular magnetization through spin–orbit torque in antiferromagnet/ferromagnet/oxide structures", *Nat. Nanotechnol.* **11**, 878 (2016).

- 15 D. MacNeill, G. M. Stiehl, M. H. D. Guimaraes, R. A. Buhrman, J. Park, and D. C. Ralph, "Control of spin-orbit torques through crystal symmetry in WTe_2 /ferromagnet bilayers", *Nature Physics* **13**, 300 (2017).
- 16 X. Chen, S. Shi, G. Shi, X. Fan, C. Song, X. Zhou, H. Bai, L. Liao, Y. Zhou, H. Zhang, A. Li, Y. Chen, X. Han, S. Jiang, Z. Zhu, H. Wu, X. Wang, D. Xue, H. Yang, and F. Pan, "Observation of the antiferromagnetic spin Hall effect", *Nat. Mater.* **20**, 800 (2021).
- 17 L. Liu, C. Zhou, X. Shu, C. Li, T. Zhao, W. Lin, J. Deng, Q. Xie, S. Chen, J. Zhou, R. Guo, H. Wang, J. Yu, S. Shi, P. Yang, S. Pennycook, A. Manchon, and J. Chen, "Symmetry-dependent field-free switching of perpendicular magnetization", *Nat. Nanotechnol.* **16**, 277 (2021).
- 18 L. Liu, C. Zhou, T. Zhao, B. Yao, J. Zhou, X. Shu, S. Chen, S. Shi, S. Xi, D. Lan, W. Lin, Q. Xie, L. Ren, Z. Luo, C. Sun, P. Yang, E.-J. Guo, Z. Dong, A. Manchon, and J. Chen, "Current-induced self-switching of perpendicular magnetization in CoPt single layer", *Nat. Commun.* **13**, 3539 (2022).
- 19 R. González-Hernández, L. Šmejkal, K. Výborný, Y. Yahagi, J. Sinova, T. Jungwirth, and J. Železný, "Efficient electrical spin splitter based on nonrelativistic collinear antiferromagnetism", *Phys. Rev. Lett.* **126**, 127701 (2021).
- 20 L. Šmejkal, J. Sinova, and T. Jungwirth, "Emerging research landscape of altermagnetism", *Phys. Rev. X* **12**, 040501 (2022).
- 21 L. Šmejkal, J. Sinova, and T. Jungwirth, "Beyond conventional ferromagnetism and antiferromagnetism: A phase with nonrelativistic spin and crystal rotation symmetry", *Phys. Rev. X* **12**, 031042 (2022).
- 22 S. Karube, T. Tanaka, D. Sugawara, N. Kadoguchi, M. Kohda, and J. Nitta, "Observation of spin-splitter torque in collinear antiferromagnetic RuO_2 ", *Phys. Rev. Lett.* **129**, 137201 (2022).
- 23 A. Bose, N. J. Schreiber, R. Jain, D.-F. Shao, H. P. Nair, J. Sun, X. S. Zhang, D. A. Muller, E. Y. Tsymbal, D. G. Schlom, and D. C. Ralph, "Tilted spin current generated by the collinear antiferromagnet ruthenium dioxide", *Nat. Electron.* **5**, 267 (2022).
- 24 H. Bai, Y. C. Zhang, Y. J. Zhou, P. Chen, C. H. Wan, L. Han, W. X. Zhu, S. X. Liang, Y. C. Su, X. F. Han, F. Pan, and C. Song, "Efficient spin-to-charge conversion via altermagnetic spin splitting effect in antiferromagnet RuO_2 ", *Phys. Rev. Lett.* **130**, 216701 (2023).
- 25 Y. Fan, Q. Wang, W. Wang, D. Wang, Q. Huang, Z. Wang, X. Han, Y. Chen, L. Bai, S. Yan, and Y. Tian, "Robust magnetic-field-free perpendicular magnetization switching by manipulating spin polarization direction in RuO_2 /[Pt/Co/Pt] heterojunctions", *ACS Nano* **18**, 26350 (2024).
- 26 M. Hiraiishi, H. Okabe, A. Koda, R. Kadono, T. Muroi, D. Hirai, and Z. Hiroi, "Nonmagnetic ground state in RuO_2 revealed by Muon Spin Rotation", *Phys. Rev. Lett.* **132**, 166702 (2024).
- 27 Z. Q. Wang, Z. Q. Li, L. Sun, Z. Y. Zhang, K. He, H. Niu, J. Cheng, M. Yang, X. Yang, G. Chen, Z. Yuan, H. F. Ding, and B. F. Miao, "Inverse spin Hall effect dominated spin-charge conversion in (101) and (110)-oriented RuO_2 films", *Phys. Rev. Lett.* **133**, 046701 (2024).
- 28 C. Wan, X. Zhang, Z. Yuan, C. Fang, W. Kong, Q. Zhang, H. Wu, U. Khan, and X. Han, "Programmable spin logic based on spin Hall effect in a single device", *Adv. Electron. Mater.* **3**, 1600282 (2017).
- 29 Y. Cui, Z. Li, H. Chen, Y. Wu, Y. Chen, K. Pei, T. Wu, N. Xie, R. Che, X. Qiu, Y. Liu, Z. Yuan, and Y. Wu, "Antisymmetric planar Hall effect in rutile oxide films induced by the Lorentz force", *Sci. Bull.* **69**, 2362 (2024).
- 30 C. Zhou, J. Xu, T. Wu, and Y. Wu, "Perspective on imaging antiferromagnetic domains in thin

- films with the magneto-optical birefringence effect", *APL Materials* **11**, 080902 (2023).
- 31 T. Wu, H. Chen, T. Ma, J. Xu, and Y. Wu, "Current-density-modulated antiferromagnetic domain switching revealed by optical imaging in the Pt/CoO(001) bilayer", *Phys. Rev. Appl.* **21**, 044054 (2024).
- 32 Y.-C. Lau, D. Betto, K. Rode, J. M. D. Coey, and P. Stamenov, "Spin-orbit torque switching without an external field using interlayer exchange coupling", *Nat. Nanotechnol.* **11**, 758 (2016).
- 33 Z. Zheng, Y. Zhang, V. Lopez-Dominguez, L. Sánchez-Tejerina, J. Shi, X. Feng, L. Chen, Z. Wang, Z. Zhang, K. Zhang, B. Hong, Y. Xu, Y. Zhang, M. Carpentieri, A. Fert, G. Finocchio, W. Zhao, and P. Khalili Amiri, "Field-free spin-orbit torque-induced switching of perpendicular magnetization in a ferrimagnetic layer with a vertical composition gradient", *Nat. Commun.* **12**, 4555 (2021).
- 34 J. Ryu, C. O. Avci, M. Song, M. Huang, R. Thompson, J. Yang, S. Ko, S. Karube, N. Tezuka, M. Kohda, K.-J. Kim, G. S. D. Beach, and J. Nitta, "Deterministic current-induced perpendicular switching in epitaxial Co/Pt layers without an external field", *Adv. Funct. Mater.* **33**, 2209693 (2023).
- 35 Y. Wu, Y. Cui, T. Wu, K. Pei, H. Chen, H. Xu, W. Qin, T. Ma, R. Che, Z. Yuan, and Y. Wu, "Perpendicular magnetic anisotropy in permalloy ultrathin film grown on RuO₂(101) surface", *Appl. Phys. Lett.* **124** (2024).
- 36 L. You, O. Lee, D. Bhowmik, D. Labanowski, J. Hong, J. Bokor, and S. Salahuddin, "Switching of perpendicularly polarized nanomagnets with spin orbit torque without an external magnetic field by engineering a tilted anisotropy", *Proc. Natl. Acad. Sci. U. S. A.* **112**, 10310 (2015).
- 37 Y. Luo, M. Liang, Z. Feng, H. Chen, N. Jiang, J. Chen, M. Yuan, J. Zhang, Y. Cheng, L. Sun, R. Bai, X. Miao, N. Wang, Y. Wu, and R. Che, "Full-scale field-free spin-orbit switching of the CoPt layer grown on vicinal substrates", *arXiv:2306.02616* (2023).
- 38 F. Wang, X. Zhang, Z. Zhang, and Y. Liu, "Deterministic magnetization switching by spin-orbit torque in a ferromagnet with tilted magnetic anisotropy: A macrospin modeling", *J. Magn. Magn. Mater.* **527**, 167757 (2021).
- 39 G. Chen, J. Li, F. Z. Liu, J. Zhu, Y. He, J. Wu, Z. Q. Qiu, and Y. Z. Wu, "Four-fold magnetic anisotropy induced by the antiferromagnetic order in FeMn/Co/Cu(001) system", *J. Appl. Phys.* **108**, 073905 (2010).
- 40 G. Chen, J. Zhu, J. Li, F. Z. Liu, and Y. Z. Wu, "Revealing the volume magnetic anisotropy of Fe films epitaxied on GaAs(001) surface", *Appl. Phys. Lett.* **98**, 132505 (2011).
- 41 C. Zhou, J. Xu, and Y. Wu, "Giant interfacial in-plane magnetic anisotropy in Co/Pt bilayers grown on MgO(110) substrates", *Physical Review Materials* **8**, 024408 (2024).
- 42 X. Zhan, H. Wang, Z. Li, and R. Liu, "Significant enhancement of spin-orbit torque efficiency by optimizing the interlayer thickness in [Pt/Ru]_n/Pt multilayers", *Appl. Phys. Lett.* **124**, 072406 (2024).

Figure 1

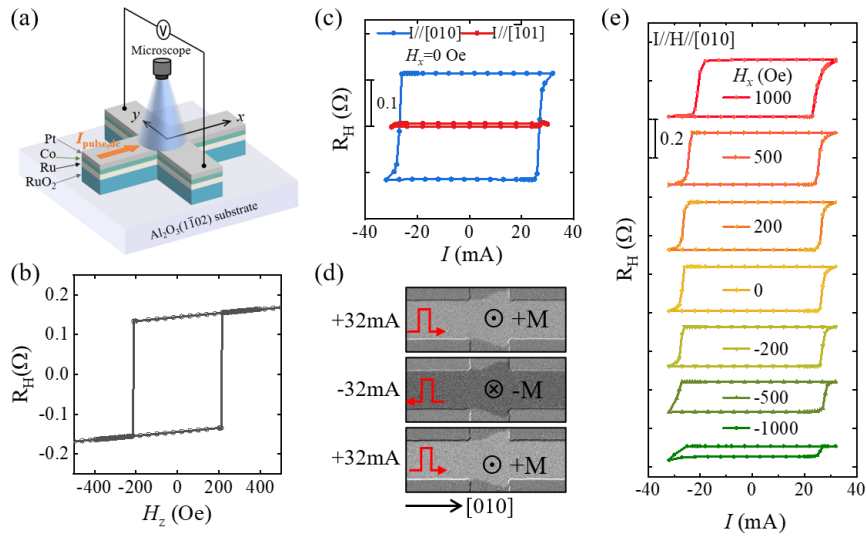


Fig. 1. (a) Experimental geometry for the current-induced switching measurement utilizing a Kerr microscope. (b) Representative AHE hysteresis loop for the Pt(2 nm)/Co(0.8 nm)/Ru(0.8 nm)/RuO₂(8 nm)/Al₂O₃(sub.) sample. (c) Current-induced magnetization switching loops measured at zero field with current applied along the [010] and $[\bar{1}01]$ directions. (d) Typical domain images captured after injecting current pulses in the [010] direction, demonstrating the full deterministic current-induced magnetization switching. (e) Current-induced magnetization switching loops assisted by in-plane magnetic fields of various amplitudes and directions.

Figure 2

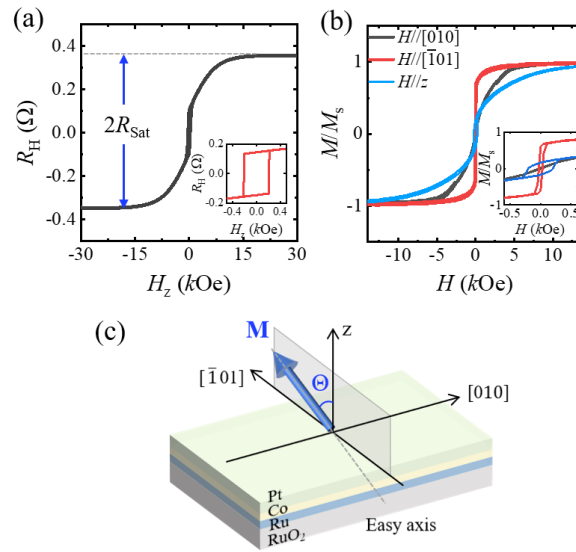


Fig. 2. (a) The typical AHE hysteresis loop of the Pt/Co/Ru/RuO₂ multilayer stack measured over a broad magnetic field range. The inset shows the loop measured over a narrow field range. (b) Out-of-plane ($H//z$ axis) and in-plane ($H//[010]$ and $H//[\bar{1}01]$) magnetic hysteresis loops for the Pt/Co/Ru/RuO₂ film. The inset indicates the loops in a narrow field range. (c) Schematic representation of the magnetic easy axis orientation in the Co layer, illustrating that it is tilted away from the z-axis towards the RuO₂ $[\bar{1}01]$ direction.

Figure 3

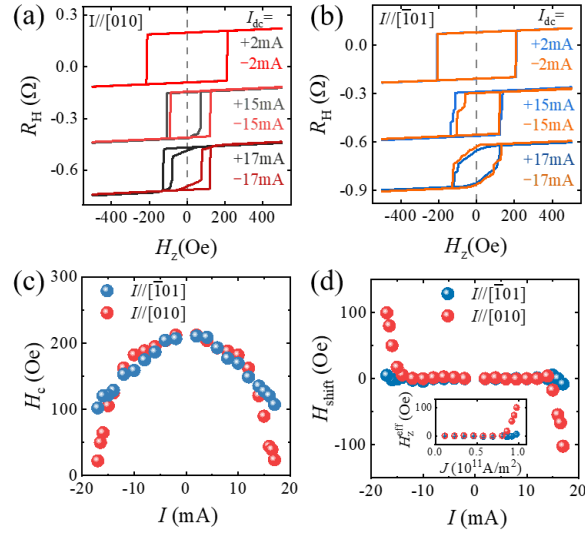


Fig. 3. (a) and (b) Hysteresis loops under $\pm I$ for (a) $I//\text{RuO}_2[010]$ and (b) $I//\text{RuO}_2[\bar{1}01]$, respectively. (c) Variation of the coercive field with the DC currents applied along two directions. (d) Current dependence of the out-of-plane effective field for currents in the $[010]$ (black dot) and $[\bar{1}01]$ (red dot) directions. H_{shift} is estimated from the loop shift in (a) and (b). The inset shows the out-of-plane effective field H_z^{eff} as a function of current density.

Figure 4

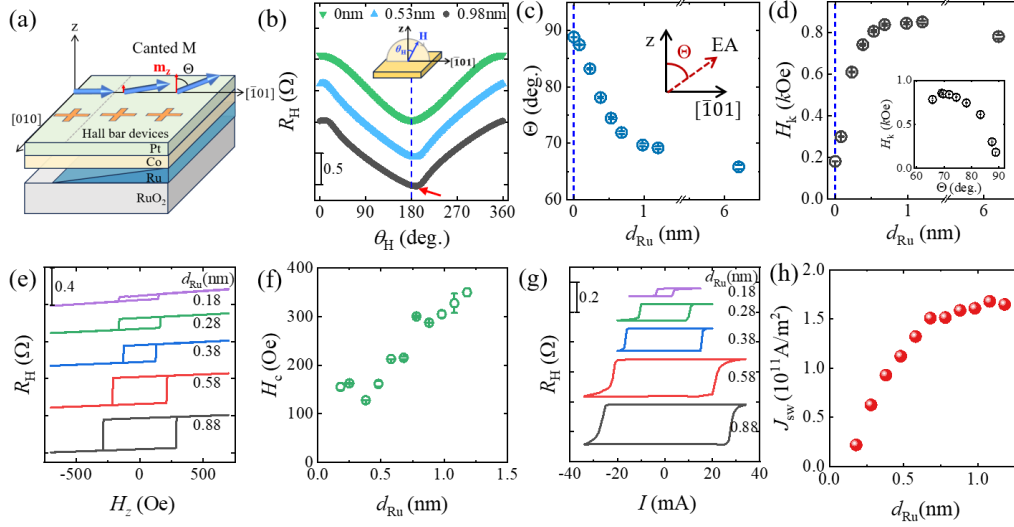


Fig. 4. (a) Schematic drawing of the Pt(2nm)/Co(0.8nm)/Ru(d_{Ru})/RuO₂(8 nm)/Al₂O₃(sub.) sample structure with the Ru layer grown into the wedged shape. The canting angle of the magnetic anisotropy also gradually changes with d_{Ru} . (b) Typical θ_H -dependent AHE signals for different d_{Ru} . The red arrow highlights that the maximum AHE signal occurs at the field angle away from z-axis. (c) Relationship between d_{Ru} and the corresponding tilt angle Θ . (d) Dependence of anisotropy field H_k on d_{Ru} . The inset shows H_k as a function of Θ . (e) Typical AHE loops for devices with varying d_{Ru} . (f) H_c as a function of d_{Ru} , extracted from the AHE loops in (e). (g) Current-induced magnetization switching loops at the zero-field condition for the devices with different d_{Ru} . (h) Critical switching current density J_{sw} as a function of d_{Ru} .